
FRUITS: Feature Extraction Using Iterated Sums for Time Series Classification

Joscha Diehl
 Universität Greifswald
 Institut für Mathematik und Informatik
 joscha.diehl@uni-greifswald.de

Richard Krieg
 Universität Greifswald
 Institut für Mathematik und Informatik
 s-rikrie@uni-greifswald.de

Abstract

We introduce a pipeline for time series classification that extracts features based on the iterated-sums signature (ISS) and then applies a linear classifier. These features are intrinsically nonlinear, capture chronological information, and, under certain settings, are invariant to time-warping. We are competitive with state-of-the-art methods on the UCR archive, both in terms of accuracy and speed. We make our code available at <https://github.com/irkri/fruits>.

Contents

1	Introduction	2
2	The iterated-sums signature	3
2.1	Iterated sums over the reals	3
2.2	Iterated sums over semirings	4
2.3	Computational complexity	5
2.4	Weighted iterated sums	6
3	FRUITS pipeline	7
3.1	Preparation	8
3.2	Iterated sums	9
3.3	Feature sieving	9
4	Experiments	10
4.1	Results on specific datasets	10
4.2	General-Purpose Fruit	12
4.2.1	Preparation	12
4.2.2	ISS Configurations	12
4.2.3	Feature Sieve Selection	14
4.3	Time warping invariance	14
4.4	A reduced pipeline	15

5 Outlook	15
A Iterated-sums signature	18
B Argmax indices	20
C Detailed results on the UCR archive	20

1 Introduction

Time series classification is a fundamental problem in data science. It has a wide range of applications [KMN08; MSS13; Zhe+14].

Deep learning methods have made significant progress in this area [WYO17; Ism+19]. But more “classical” methods are still competitive / SOTA, [Bag+17; DPW20; Mid+21; Tan+22; DSW23; MSB23] with the added benefits of simplicity and speed.

In this paper, we present a pipeline for time series classification that extracts features based on the iterated-sums signature (ISS) [DET20; DET22] and then applies a linear classifier. The pipeline is called FRUITS (Feature Extraction Using Iterated Sums), and its two-stage approach is similar to the one of the Rocket [DPW20] pipeline.

The substantial difference is that **FRUITS’ iterated sums are nonlinear to begin with**, whereas Rocket uses random *linear* convolutions (and achieves nonlinearity through pooling operations before the linear classifier).

We achieve competitive results on the UCR archive [Dau+19], and, for choices of hyperparameters, time-warping invariance.

Iterated sums and integrals in data science Let $x : \mathbb{N} \rightarrow \mathbb{R}$ be a one-dimensional time series. Iterated sums are (mostly nonlinear) transformations of x obtained by summing certain polynomial expressions of its past values. Simple examples are

$$\sum_i x_i, \quad \sum_{t_1 < t_2} x_{t_1} x_{t_2}, \quad \sum_{t_1 < t_2} x_{t_1}^2 x_{t_2}.$$

Note that the first sum here is linear in x (it is the only linear “iterated” sum). It is well-known that a simple sum of this type is invariant to arbitrary permutations of the time steps (leading, for example, to their use in deep sets [Zah+17]). We note that the second sum, which is an honest *iterated* sum, namely

$$\sum_{t_2} \left(\sum_{t_1 < t_2} x_{t_1} \right) x_{t_2},$$

is also invariant to arbitrary permutations of the time steps. The third one is *not* and it therefore truly captures some sort of “chronological” information.

Iterated sums in general *are* invariant to arbitrarily inserting zeros into a sequence. This invariance played a key role in their development and is one of their most important properties, [DET20; DET22]. When applying iterated sums to the *increments* $\delta x_i = x_i - x_{i-1}$, it yields invariance to “stuttering” or repetition of values, and hence an invariance to time-warping. Such time-warping invariance is important in many applications, as evidenced by the extensive literature on dynamic time warping (DTW) [BC94; YJF98; KR05; CB17].

Another perspective on iterated sums is considering them a discretization of *iterated integrals*. These features of continuous-time curves date back to Chen’s work on the homology of path spaces [Che57] and have been used in the last decades in control theory [Fli81], rough path analysis [Lyo98] and, more recently, data science [Xie+17; CNO18; DR19; Kid+19; KO19; Kid+20; Cuc+21]. We note that applying iterated integrals to a one-dimensional time series results in trivial features (owing to the fundamental theorem of calculus). This well-known problem is usually circumvented by first lifting the time series to a higher-dimensional space, for example by adding a time-dimension. The

ISS does *not* necessitate such a lift, as it provides a huge variety of nonlinear features already in one dimension.

Contributions We provide, for the first time, a comprehensive study of the use of the iterated-sums signature (ISS) as a feature-extraction method for time series classification. We restrict to a “classical”, non-deep learning setting: the features are not learned, but computed from the data and then used in a linear classifier. This is accompanied by a fast implementation of the ISS, in a well-documented and unit-tested Python package, <https://github.com/irkri/fruits>.

We show that our method is competitive with state-of-the-art methods on the UCR archive, while providing additional benefits such as being deterministic, and providing for certain choices of hyperparameters, time-warping invariance.

Moreover, we develop the ISS in the following directions:

- We introduce a weighting scheme for the ISS that penalizes/boosts summands depending on the distance of their indices. This idea appeared in [Kri21] for the first time, and we extend it to new weighting schemes that bear close resemblance to positional encodings in NLP [Vas+17].
- In the arctic semiring, in addition to the iterated sums, which yield certain *values* at global maxima/minima, we provide a linear-in-time algorithm to also obtain the *indices*.

Outline In Section 2, we introduce the ISS and its generalization to semirings. In Section 3 we describe our pipeline, that uses the ISS as the central feature extractor. In Section 4, we present our experiments.

The appendix contains a more detailed introduction to the ISS and an algorithm to obtain the indices of the global maxima/minima that is mentioned in Section 2.2.

2 The iterated-sums signature

$\mathbb{N} = \{0, 1, \dots\}$ denotes the non-negative integers, and $\mathbb{N}_{\geq 1} = \{1, 2, \dots\}$ the positive integers.

We will denote a d -dimensional time series by a lowercase letter $x \in \mathcal{Z}_d$ and interpret it as a function on the natural numbers,

$$\mathcal{Z}_d := \{x \mid x : \mathbb{N}_{\geq 1} \rightarrow \mathbb{R}^d\}.$$

The collection of time series of length T will be denoted by

$$\mathcal{Z}_d|_T := \{x \mid x : \{1, \dots, T\} \rightarrow \mathbb{R}^d\}.$$

We write $x_t = x(t) \in \mathbb{R}^d$ for a single time step $t \in \mathbb{N}_{\geq 1}$. Entries of this d -dimensional vector are accessed using a superscript $x_t^{[j]}$ for $j \in \{\mathbf{1}, \dots, \mathbf{d}\}$. We extend this notation to formal, commutative monomials of the indices, e.g. $x_t^{[1^2 3]} = x_t^{[1]} x_t^{[1]} x_t^{[3]}$.

2.1 Iterated sums over the reals

The **iterated-sums signature (ISS)** was first introduced, in an algebraic framework, in [DET20]. We sketch its construction here, more details can be found in Appendix A.

The ISS consists of polynomial expressions in the time series’ values, indexed by **words** $w = [a_1] \dots [a_p]$. Here, a **letter** $[a_i]$ is a non-constant monomial in the dummy variables $\mathbf{1}, \dots, \mathbf{d}$ (in other words $[a_i] \in \mathbb{N}^d$, with at least one non-zero entry). The total number of those variables in a word w is called its **weight** $|w|$. For a fixed word w we obtain a new (one-dimensional) time series, $\text{ISS}_w(x) \in \mathcal{Z}_1$, where the value at each time step is an iterated sum of the input signal’s past as follows

$$\text{ISS}_w(x)_t := \sum_{0 < t_1 < \dots < t_p \leq t} x_{t_1}^{[a_1]} \dots x_{t_p}^{[a_p]}. \quad (1)$$

For example, for a two-dimensional time series $x \in \mathcal{Z}_2|_T$ and the word $w = [1^2 2][2^3]$ we have

$$\text{ISS}_{[1^2 2][2^3]}(x)_t = \sum_{0 < t_1 < t_2 \leq t} x_{t_1}^{[1^2 2]} \cdot x_{t_2}^{[2^3]} = \sum_{0 < t_1 < t_2 \leq t} \left(x_{t_1}^{[1]}\right)^2 x_{t_1}^{[2]} \left(x_{t_2}^{[2]}\right)^3.$$

i.e. formal products in a_i translate to products of the corresponding dimensions at coinciding time step in the iterated sum. The ISS therefore allows different time steps as well as dimensions in a time series to interact, non-linearly, with each other.

2.2 Iterated sums over semirings

Semirings are algebraic structures that generalize rings by dropping the requirement of additive inverses. They appear for example in theoretical computer science, where they are used in automata theory and in describing certain dynamic programming algorithms, [Moh+02].

Diehl et al. [DET22] show that the ISS can actually be defined over arbitrary commutative semirings, another fact that distinguishes it from iterated integrals. A **commutative semiring** \mathbb{S} is a tuple $(S, \oplus, \odot, \mathbb{0}, \mathbb{1})$ where

- S is a set,
- $\oplus : S \times S \rightarrow S$ is associative, commutative and $\mathbb{0} \oplus s = s$ for all $s \in S$,
- $\odot : S \times S \rightarrow S$ is associative, commutative and $\mathbb{1} \odot s = s$ for all $s \in S$ and
- $\mathbb{0} \odot s = s \odot \mathbb{0} = \mathbb{0}$ for all $s \in S$.

Every commutative ring is a commutative semiring. For the commutative ring of real numbers $\mathbb{S}_{\mathbb{R}} = (\mathbb{R}, +, \cdot, 0, 1)$ the iterated-sums signature is already introduced in Section 2.1. Replacing the standard sum and product of that definition by the operations in a commutative semiring \mathbb{S} , we obtain the following definition

$$\begin{aligned} \text{ISS}_w^{\mathbb{S}} : \mathcal{Z}_d &\rightarrow \mathcal{Z}_1 \\ \text{ISS}_w^{\mathbb{S}}(x)_t &= \bigoplus_{0 < t_1 < \dots < t_p \leq t} x_{t_1}^{\odot[a_1]} \odot \dots \odot x_{t_p}^{\odot[a_p]} \end{aligned} \quad (2)$$

for some word $w = [a_1] \dots [a_p]$. The symbol \odot in the exponent $x_{t_j}^{\odot[a_j]}$ now highlights that a formal product of dimension indices in a_j translates to repeatedly applying \odot .

Arctic iterated sums The canonical example of a commutative semiring that is *not* a ring is the **arctic** (or **max-plus**) semiring $\mathbb{S}_{\mathbb{A}} = (\mathbb{R} \cup \{-\text{inf}\}, \max, +, -\text{inf}, 0)$.¹ As an example, let $w = [1][1^2][23]$ and $x \in \mathcal{Z}_3|_T$. We then have,

$$\begin{aligned} \text{ISS}_w^{\mathbb{S}_{\mathbb{A}}}(x)_T &= \max_{0 < t_1 < t_2 < t_3 \leq T} x_{t_1}^{\odot[1]} + x_{t_2}^{\odot[1^2]} + x_{t_3}^{\odot[23]} \\ &= \max_{0 < t_1 < t_2 < t_3 \leq T} x_{t_1}^{[1]} + 2x_{t_2}^{[1]} + x_{t_3}^{[2]} + x_{t_3}^{[3]}. \end{aligned}$$

A real-valued time series can be considered as taking values in the arctic semiring. Calculating the corresponding (arctic) iterated sums leads to features that are quite different from the (classical, real) iterated sums. The latter are smooth, polynomial expressions whereas the former are piecewise linear expressions of cumulative maxima.

As noted in [DET22], such expressions are not time-warping invariant (but, of course, invariant to insertion of zeros, which in this case corresponds to the insertion of $-\infty$). One obtains time-warping invariant features by using non-strict inequalities for the indices. We are thus led to define

$$\begin{aligned} \underline{\text{ISS}}_w^{\mathbb{S}_{\mathbb{A}}} : \mathcal{Z}_d &\rightarrow \mathcal{Z}_1 \\ \underline{\text{ISS}}_w^{\mathbb{S}_{\mathbb{A}}}(x)_t &= \langle w, \text{ISS}_{0,t}^{\mathbb{S}_{\mathbb{A}}}(x) \rangle = \bigoplus_{1 \leq t_1 \leq \dots \leq t_p \leq t} x_{t_1}^{\odot[a_1]} \odot \dots \odot x_{t_p}^{\odot[a_p]}. \end{aligned} \quad (3)$$

¹Equivalently, one can use the **tropical** semiring $\mathbb{S}_{\mathbb{T}} = (\mathbb{R} \cup \{\text{inf}\}, \min, +, \text{inf}, 0)$.

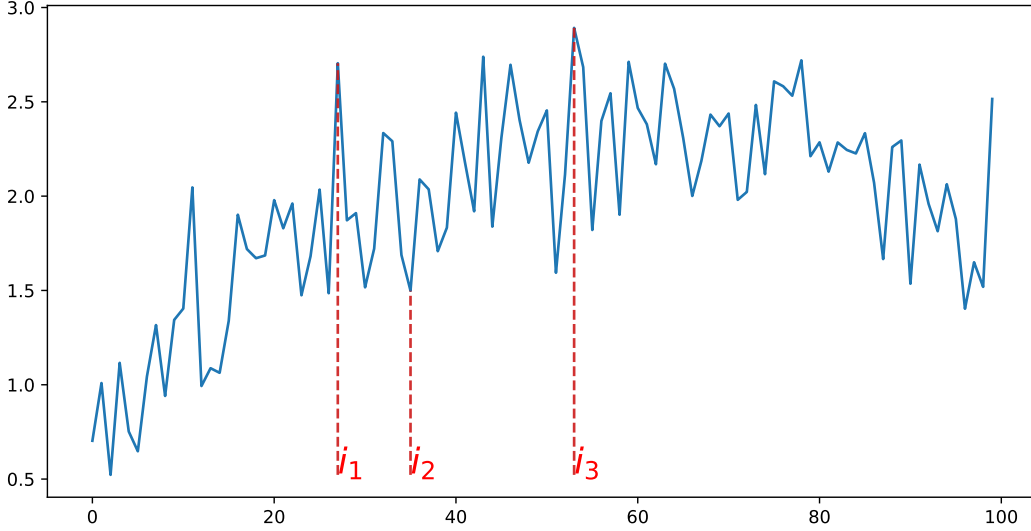


Figure 1: Indices in the arctic iterated sum $\text{ISS}_{[1][1^{-1}][1]}^{\mathbb{S}^A}(x)$ for a time series x . A linear combination of sinusoidal waves with random Gaussian noise is used.

As an example, let $w = [1][1^2][23]$ and $x \in \mathcal{Z}_3|_T$. For the arctic semiring, we now have

$$\begin{aligned}
 \text{ISS}_w^{\mathbb{S}^A}(x)_T &= \max_{1 \leq t_1 \leq t_2 \leq t_3 \leq T} x_{t_1}^{\odot[1]} + x_{t_2}^{\odot[1^2]} + x_{t_3}^{\odot[23]} \\
 &= \max_{1 \leq t_1 \leq t_2 \leq t_3 \leq T} x_{t_1}^{[1]} + 2x_{t_2}^{[1]} + x_{t_3}^{[2]} + x_{t_3}^{[3]} \\
 &= \max_{1 \leq t_1 \leq t_3 \leq T} 3x_{t_1}^{[1]} + x_{t_3}^{[2]} + x_{t_3}^{[3]} \\
 &= \text{ISS}_w^{\mathbb{S}^A}(x)_T,
 \end{aligned}$$

where $\tilde{w} = [1^3][23]$. As observed in [DET22], this phenomenon leads to a “collapse” of most of the features for these modified iterated sums. To circumvent this, we follow the suggestion in [DET22], and allow *negative* exponents $n_1, \dots, n_k \in \mathbb{Z} \setminus \{0\}$ for an extended letter $a_i = [d_1^{n_1} \dots d_k^{n_k}]$. In the arctic semiring, this leads to interesting objects. If we for example use alternating signs $w = [1^1][1^{-1}][1^1][1^{-1}] \dots$, the transformation $\text{ISS}_w^{\mathbb{S}^A}$ looks for a maximum, followed by the next minimum, followed by another maximum, and so on. The largest possible sum resulting from such constellations (where minima are multiplied by -1) is returned. Figure 1 shows an example of the indices of maxima and minima for this arctic iterated sum for a word of length 3, $w = [1][1^{-1}][1]$. One can see that naively searching for those optima may take time in $\mathcal{O}(T^3)$. Iterated sums can do this in linear time, as we will see in Section 2.3.

In the proceeding determination of the iterated sum, the *position* of the attained maxima/minima is lost, but there is a way to simultaneously keep track of them, Appendix B.

2.3 Computational complexity

While the definition in (2) seems to involve the computation of $\mathcal{O}(T^p)$ terms for the entire sum, it is a well known fact that iterated sums (and integrals) can be efficiently calculated using a simple dynamic programming principle. This reduces the complexity to $\mathcal{O}(T \cdot p)$ and is based on the following two facts, which follow from Theorem A.2 in the appendix.

For a semiring \mathbb{S} , let $\text{CS}_r^{\mathbb{S}} : \mathcal{Z}_1 \rightarrow \mathcal{Z}_1$,

$$\text{CS}_r^{\mathbb{S}}(x)_s := \begin{cases} 0 & , 1 \leq s \leq r \\ \bigoplus_{j=1}^{s-r} x_j & , s > r \end{cases},$$

be the cumulative sum with an additional “shift” $r \in \mathbb{N}$.

Fact 1. For a word $w = [a_1] \cdots [a_p]$, $p \geq 1$ and $x \in \mathcal{Z}_d$

$$\text{ISS}_w^{\mathbb{S}}(x) = \text{CS}_0^{\mathbb{S}} \left(x^{[a_p]} \odot \text{CS}_1^{\mathbb{S}} \left(x^{[a_{p-1}]} \odot \text{CS}_1^{\mathbb{S}} \left(\dots x^{[a_2]} \odot \text{CS}_1^{\mathbb{S}}(x^{[a_1]}) \right) \right) \right),$$

where “ \odot ” stands for the entry-wise product of time series in \mathbb{S} .

When dealing with iterated sums that have non-strict index inequalities (3), a slight modification can be made.

Fact 2. For a word $w = [a_1] \cdots [a_p]$, $p \geq 1$ and $x \in \mathcal{Z}_d$

$$\underline{\text{ISS}}_w^{\mathbb{S}}(x) = \text{CS}_0^{\mathbb{S}} \left(x^{\odot[a_p]} \odot \text{CS}_0^{\mathbb{S}} \left(x^{\odot[a_{p-1}]} \odot \text{CS}_0^{\mathbb{S}} \left(\dots x^{\odot[a_2]} \odot \text{CS}_0^{\mathbb{S}}(x^{\odot[a_1]}) \right) \right) \right), \quad (4)$$

where “ \odot ” stands for the entry-wise product of time series in \mathbb{S} .

2.4 Weighted iterated sums

Different weighting of information at different time steps has been used in various applications, e.g. in RNNs [Kou+14], in transformers [Qin+21], and recently, in the context of iterated sums [Kri21] (we note related algebraic consideration in [FMZ21, p.2]).

We see in (1) that all index combinations t_1, \dots, t_p are treated equally. In many applications, however, it is desirable to give more weight to combinations of indices that are close to one another. We introduce a weighting to $\text{ISS}_w^{\mathbb{S}}$ that penalizes summands which are further apart from one another. We are thus looking for a class of functions $\omega : [T]^{p+1} \rightarrow S$, such that for the **weighted iterated sum**

$$\text{ISS}_w^{\mathbb{S}, \omega}(x)_t := \bigoplus_{0 < t_1 < \dots < t_p \leq t} \omega(t_1, \dots, t_p, t) \odot x_{t_1}^{\odot[a_1]} \odot \dots \odot x_{t_p}^{\odot[a_p]}. \quad (5)$$

- I) the calculation of the weighted iterated sum still is compatible with the dynamic programming procedure (Section 2.3), and
- II) $\omega(t_1, \dots, t_p, t)$ is decreasing as $|t_1 - t|$ increases.

For the standard semiring $\mathbb{S}_{\mathbb{R}}$ an exponential weighting of the following form fulfills these requirements. Let $g : \mathbb{N} \rightarrow \mathbb{R}$, be a non-decreasing function and define

$$\begin{aligned} \omega_{\alpha_1, \dots, \alpha_p}^{\mathbb{S}_{\mathbb{R}}}(t_1, \dots, t_p, t) &:= e^{\alpha_1(g(t_1) - g(t_2)) + \dots + \alpha_{p-1}(g(t_{p-1}) - g(t_p)) + \alpha_p(g(t_p) - g(t))} \\ &= e^{\alpha_1 g(t_1)} \cdot \left(\prod_{k=2}^p e^{(\alpha_k - \alpha_{k-1})g(t_k)} \right) \cdot e^{-\alpha_p g(t)} \end{aligned}$$

for $\alpha_1, \dots, \alpha_p \geq 0$ as a weighting on $\mathbb{S}_{\mathbb{R}}$. For example, with $g(x) = x$, $\alpha_1, \alpha_2, \alpha_3 > 0$, and for a word of length 3, $w = [a_1][a_2][a_3]$ and $x \in \mathcal{Z}_d|_T$ we obtain the weighted iterated sum

$$\sum_{0 < t_1 < t_2 < t_3 \leq T} e^{\alpha_1(t_1 - t_2) + \alpha_2(t_2 - t_3) + \alpha_3(t_3 - T)} x_{t_1}^{[a_1]} x_{t_2}^{[a_2]} x_{t_3}^{[a_3]}.$$

Addition in the exponent becomes a multiplication of exponentials. Hence, with the definition

$$y_{t_k} := \exp((\alpha_k - \alpha_{k-1})g(t_k)) x_{t_k}^{[a_k]} \text{ for } k = 1, \dots, p \quad (6)$$

where $\alpha_0 = 0$, one can verify that the formula of Proposition 1 still holds for the weighted iterated sum

$$\text{ISS}_w^{\mathbb{S}_{\mathbb{R}}, \omega_{\alpha_1, \dots, \alpha_p}^{\mathbb{S}_{\mathbb{R}}}}(x) = \nu \cdot \text{CS}_0^{\mathbb{S}_{\mathbb{R}}} \left(y^{[a_p]} \cdot \text{CS}_1^{\mathbb{S}_{\mathbb{R}}} \left(y^{[a_{p-1}]} \cdot \text{CS}_1^{\mathbb{S}_{\mathbb{R}}} \left(\dots y^{[a_2]} \cdot \text{CS}_1^{\mathbb{S}_{\mathbb{R}}}(y^{[a_1]}) \right) \right) \right)$$

with $\nu = (e^{-\alpha_p \cdot 1}, \dots, e^{-\alpha_p \cdot T})$.

For the arctic semiring, this argument does not work, as $\omega^{\mathbb{S}_{\mathbb{R}}}$ does not fulfill I). We instead use

$$\omega_{\alpha_1, \dots, \alpha_p}^{\mathbb{S}_{\mathbb{A}}}(t_1, \dots, t_p, t) := \alpha_1 \cdot (g(t_1) - g(t_2)) + \dots + \alpha_p \cdot (g(t_p) - g(t)),$$

which allows to repeat the argument above for $y_{t_k} = (\alpha_k - \alpha_{k-1})g(t_k) + x_{t_k}^{\odot[a_k]}$ and an appropriate “additive” ν .

In either case, the function g can actually depend on the time series x , and we can choose it of the form

$$g(t) := f(h(t, x)), \text{ where } f : [0, 1] \rightarrow \mathbb{R}, h : \mathbb{N} \times \mathcal{Z}_d|_T \rightarrow [0, 1]. \quad (7)$$

We experiment with different h , e.g. the (normalized) sum of absolute increments²

$$h^{(L1)}(t, x) := \frac{\sum_{r=2}^t |\delta x_r|}{\sum_{r'=2}^T |\delta x_{r'}|} \quad (8)$$

or the sum of squared increments $h^{(L2)}$. However, contrary to our initial beliefs, setting $h^{(id)}(t, x) = \frac{t}{T}$ works best on the UCR archive.

The scaling function f is chosen such that the weights have a non-vanishing impact in the overall iterated sum. As the exponential often leads to exploding values, we restrict the range of the weights to $[0, 50]$, i.e. $f(x) = 50x$.

In our experiments we will set $\alpha_1 = \dots = \alpha_{p-1} = 1$, so that the summands of the ISS are just penalized over the total time range they cover, as the sum of distances in the exponents becomes a telescoping sum. We will use the shorter notation $\text{ISS}_w^{\mathbb{S}, \omega} = \text{ISS}_w^{\mathbb{S}, \omega_{1, \dots, 1}}$.

Periodic Weightings Allowing complex numbers $\gamma \in \mathbb{C}$ in the exponent $e^{\gamma(t_1 - t_2)}$ allows for periodical weightings. We explore cosine weightings, which is a special case of that form and is easier to handle. In the standard semiring $\mathbb{S}_\mathbb{R}$, this weighting is defined by

$$\omega_f^{\cos^b}(t_1, \dots, t_p, t) = \prod_{k=2}^p \cos(\alpha_{k-1}(t_{k-1} - t_k))^b \cdot \cos(\alpha_p(t_p - t))^b,$$

where $b \in \mathbb{N}$. We set the scalars $\alpha_1 = \dots = \alpha_p = \frac{\pi}{f \cdot T}$ and $f \in [0, 1]$ is a frequency parameter. For a word of length two and $b = 1$, we can use the trigonometric identity $\cos(a - b) = \cos(a)\cos(b) + \sin(a)\sin(b)$ in

$$\begin{aligned} \text{ISS}_{[1][1]}^{\omega_f^{\cos}}(x)_t &= \sum_{0 < t_1 < t_2 \leq t} \cos(\alpha_1(t_1 - t_2))\cos(\alpha_2(t_2 - t))x_{t_1}x_{t_2} \\ &= \sum_{0 < t_1 < t_2 \leq t} (\cos(\alpha_1 t_1)\cos(\alpha_1 t_2) + \sin(\alpha_1 t_1)\sin(\alpha_1 t_2)) \\ &\quad \cdot (\cos(\alpha_2 t_2)\cos(\alpha_2 t) + \sin(\alpha_2 t_2)\sin(\alpha_2 t))x_{t_1}x_{t_2} \\ &= \sum_{0 < t_1 < t_2 \leq t} \cos(\alpha_1 t_1)\cos(\alpha_1 t_2)\cos(\alpha_2 t_2)\cos(\alpha_2 t)x_1 x_2 \\ &\quad + \cos(\alpha_1 t_1)\cos(\alpha_1 t_2)\sin(\alpha_2 t_2)\sin(\alpha_2 t)x_1 x_2 \\ &\quad + \sin(\alpha_1 t_1)\sin(\alpha_1 t_2)\cos(\alpha_2 t_2)\cos(\alpha_2 t)x_1 x_2 \\ &\quad + \sin(\alpha_1 t_1)\sin(\alpha_1 t_2)\sin(\alpha_2 t_2)\sin(\alpha_2 t)x_1 x_2, \end{aligned}$$

to arrive again at an expression suited for dynamic programming. Note that this last expression is the sum of four iterated sums. It is straight-forward to write in a similar fashion, an algorithm for words of any length and arbitrary $b \in \mathbb{N}$. Cosine weighting can be thought of as a continuous version of a spacing, or dilation, operation, Figure 2.

3 FRUITS pipeline

The FRUITS pipeline comprises three steps. Each one has its own set of hyperparameters. An entire pipeline is defined by a configuration of these hyperparameters, and we will refer to one such

² $\delta x_i := x_i - x_{i-1}$; see also Section 3.1.

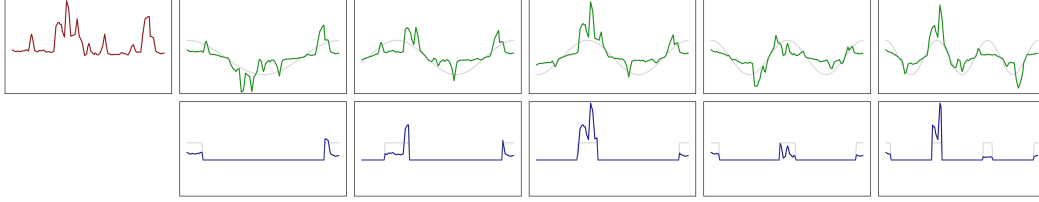


Figure 2: Example time series (red), multiplied with cosines/sines of different frequencies (green) and corresponding dilations of similar frequencies (blue). Multiplier in light gray.

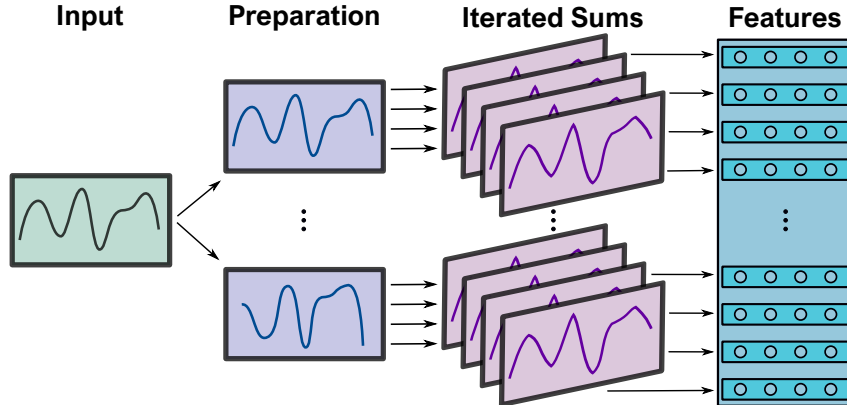


Figure 3: The FRUITS pipeline.

configuration as a “fruit”. We restrict the following discussion to the most vital parts of the pipeline. We make our code available as a Python package³. The package is written in an object-oriented programming style, which makes it easy to use and customize.

The following subsections will introduce transformations in each of the three steps of the FRUITS pipeline, Figure 3. First, FRUITS will preprocess the input data in the “preparation step”. These transformations, introduced in Section 3.1 will be called *prepareurs*. After preparation, the iterated sums for different semirings, words and weighting configurations are calculated. The result of this second step is a (family of) transformed one-dimensional time series. The last step then extract features from these time series, a process we call *sieving*. The transformations here will be called *feature sieves*.

3.1 Preparation

The data preparation stage preprocesses the input data before the calculation of the iterated sums.

Standardization Standardization, a very common transform for machine learning pipelines, has a significant impact on the accuracy performance of FRUITS. We apply it in each of the pipelines at the very beginning, normalizing every single time series to have mean zero and standard deviation one. We also experimented with other normalizations, e.g. to the interval $[0, 1]$, but found standardization to work best.

Increments The increments of a time series,

$$\text{INC} : \mathcal{Z}_d \rightarrow \mathcal{Z}_d, x \mapsto (0, x_2 - x_1, x_3 - x_2, \dots) =: \delta x,$$

can be considered the discrete analog of a derivative. Calculating the ISS on it leads to *time-warping invariant* features $\text{ISS}_w(\delta x)_T$, see [DET20], [DET22] for an in-depth discussion. For example, two time series

$$\begin{aligned} x &= (x_1, x_2, x_3, x_4, x_5, x_6, x_7, \dots, x_{T-2}, x_{T-1}, x_T) \in \mathcal{Z}_d|_T, \\ y &= (x_1, x_2, x_3, x_3, x_3, x_4, x_5, x_6, x_7, \dots, x_{T-2}, x_{T-1}, x_T) \in \mathcal{Z}_d|_{T+2} \end{aligned}$$

³<https://github.com/irkri/fruits>

have the same feature representation using this preparateur and appropriate feature sieves. We will discuss details in Section 3.3. Here we say that y is the time series obtained by *stuttering* x at time step 3 two times.

Experiments showed that lifting a univariate time series to two dimensions, where the second dimension is given by its increments leads to a significant improvement in accuracy. We denote this preparateur map by

$$\begin{aligned} \text{INC}^\dagger : \mathcal{Z}_1 &\rightarrow \mathcal{Z}_2 \\ x = (x_1, x_2, x_3, \dots) &\mapsto \left(\begin{pmatrix} x_1 \\ 0 \end{pmatrix}, \begin{pmatrix} x_2 \\ x_2 - x_1 \end{pmatrix}, \begin{pmatrix} x_3 \\ x_3 - x_2 \end{pmatrix}, \dots \right). \end{aligned} \quad (9)$$

Further down the pipeline, using words over an alphabet with two dimensions $A = \{1, 2\}$, we get interesting expressions like

$$\text{ISS}_{[12]}(\text{INC}^\dagger(x))_T = \sum_{t \leq T} x_i(x_i - x_{t-1}) = \sum_{t \leq T} x_t^2 - x_t x_{t-1} = \text{ISS}_{[11]}(x)_T - \sum_{t \leq T} x_t x_{t-1}.$$

The second term cannot be easily approximated by linear transformations on iterated sums of just x . However, we want to note that it can be approximated by choosing an appropriate weighting control function g , see (7). We only need to ensure $e^{g(t_1) - g(t_2)} \approx 0$ for $|t_1 - t_2| > 1$.

3.2 Iterated sums

The central part of FRUITS, the iterated-sums signature ISS, is applied to the preprocessed time series, obtained from one or multiple preparateurs presented in Section 3.1. Several options can be considered for the ISS.

1. The words the ISS is calculated for.
2. The semiring in which the operations \oplus, \odot are performed.
3. The type of weighting we apply to the signature.

Experiments suggesting the best options are presented in Section 4.

3.3 Feature sieving

The output of $\text{ISS}_w(x)$ is a one-dimensional time series $z \in \mathcal{Z}_1|_T$ of the same length T as the input $x \in \mathcal{Z}_d|_T$. Using a preselected set of words w , we get a number of iterated sums for each sample in the dataset. We will now extract representative features from the iterated sums, a process we call *sieving*. As the calculation of iterated sums for a large number of words is expensive, extracting several meaningful features from each iterated sum reduces computation costs and increases feature variety.

Last value A natural feature for $x \in \mathcal{Z}_d|_T$ is the total iterated sum $\text{ISS}_w^{\mathbb{S}}(x)_T$, the corresponding feature sieve is named $\text{END} : z \mapsto z_T$. The entire input time series is considered for this feature.

Coquantiles We can also cut the time series at some time $s < T$, i.e. considering a sieve $z \mapsto z_s$. To again get time-warping invariant features, we introduce *coquantiles*. For a given $0 < q < 1$ we define

$$\zeta_q^G(x) := \max \{t \in \{1, \dots, T\} \mid (G(\delta x))_t \leq q \cdot \sup(G(\delta x))\}$$

for a function $G : \mathcal{Z}_d|_T \rightarrow \mathcal{Z}_1|_T$ returning monotonic increasing time series. We set $\zeta_0^w(x) := 1$ and $\zeta_1^w(x) := T$. A natural choice is

$$\zeta_q^{h^{(L1)}}(x) = \max \left\{ t \in \{1, \dots, T\} \mid h^{(L1)}(t) \leq q \right\}$$

where $G = h^{(L1)}$, see (8). For this choice,

$$\text{ISS}_w^{\mathbb{S}}(y)_{\zeta_q^G},$$

is invariant under stuttering. However, experiments on the UCR archive show that coquantiles do not lead to a better performance of our pipelines. We will omit them in later discussions and leave this paragraph as a remark.

Number of positive increments Dempster et al. [DPW20] found that for ROCKET, the feature *Proportion of Positive Values (PPV)* is essential for their good performance. Loosely speaking, this transform calculates the relative number of occurrences of a certain pattern in a time series. In the case of ROCKET, this pattern is given by a (randomized) kernel. The performance of PPV highly depends on a good choice of a reference value, for which numbers greater than this value are considered “positive”. In ROCKET, this reference value is a quantile of a convolution of one sample in the training dataset.

Inspired by this, FRUITS calculates the *Number of Positive Increments* $\text{NPI} : \mathcal{Z}_1 \rightarrow [0, 1]$,

$$\text{NPI}(z) := \sum_{t=1}^T \mathbb{1}_{\text{INC}(z)_t > 0} \text{ where } \mathbb{1}_{a > 0} = \begin{cases} 0, & a \leq 0 \\ 1, & a > 0 \end{cases},$$

which is the number of time steps for which the z is increasing. We note that this sieve is automatically time-warping invariant. One immediate consequence of the definition is that we get constant values $\text{NPI}(z) \in \mathcal{O}(T)$ for strictly monotonically increasing iterated sums $z = \text{ISS}_w^{\mathbb{S}}(y)$, e.g. for $w = [11], w = [1111], w = [11][11]$ (we write $\mathcal{O}(T)$ as the actual result depends on the length of w). We generalize NPI to k -th order increments $\text{INC}^k(z) = \text{INC}(\text{INC}(\dots \text{INC}(z)))$ (k -times) and write

$$\text{NPI}^k(z) := \sum_{t=1}^T \mathbb{1}_{\text{INC}^k(z)_t > 0}$$

with the special case $\text{NPI}^0(z) = T \cdot \text{PPV}(z)$. Additionally, we restrict NPI to only count positive increments in a certain window

$$\text{NPI}_{\alpha_l, \alpha_r}^k(z) := \sum_{t=1}^T \mathbb{1}_{q_l < \text{INC}^k(z)_t \leq q_r}.$$

This window is given by quantiles q_l and q_r , which are the estimated α_l - and α_r -quantiles of the iterated sums of samples from the training set. In most experiments we set $\alpha_l = 0.5$ and $\alpha_r = 1$, for which we define $q_r = \infty$.

Using the arctic semiring $\mathbb{S} = \mathbb{S}_A$, $\text{NPI}(\text{ISS}_w^{\mathbb{S}_A}(y))$ counts the number of times the outer maximum of the iterated sum

$$\max_{1 \leq t_1 \leq \dots \leq t_p \leq T} y_{t_1}^{\odot [a_1]} + \dots + y_{t_p}^{\odot [a_p]} \text{ for } w = [a_1] \dots [a_p]$$

changes. $\text{NPI}^2(\text{ISS}_w^{\mathbb{S}_A}(y))$ on the other hand has a less intuitive interpretation. It counts how often small changes are followed by larger changes of this maximum. Experiments show that this feature sieve, for both the standard as well as the arctic semiring boost the performance of the pipeline.

Mean of positive increments MULTIROCKET [DSW21] also introduces variations of PPV to the ROCKET pipeline. We found that one such variation also improves the performance of FRUITS. Similarly to NPI, we change the MPV operation from MULTIROCKET to

$$\text{MPI}_{\alpha_l, \alpha_r}^k(z) := \frac{1}{T} \sum_{t=1}^T \mathbb{1}_{q_l < \text{INC}^k(z)_t \leq q_r} \text{INC}^k(z)_t,$$

which is the mean of positive increments in a window restricted by estimated quantiles.

4 Experiments

We conduct extensive experiments on the datasets in the UCR-archive [Dau+19]. We will use a linear regression classifier with L2 regularization in all experiments, the same classifier used in ROCKET [DPW20]. Using cross-validation, a suitable regularization parameter can be found quickly for this ridge regression.

4.1 Results on specific datasets

This section presents novel observations we made on several datasets from the UCR archive, some of which motivate certain choices we made for the FRUITS pipeline.

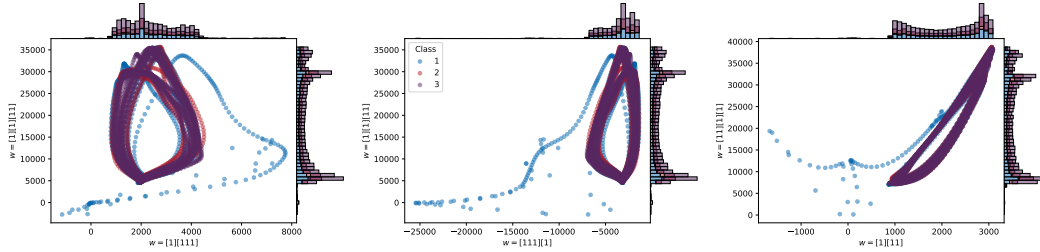


Figure 4: Scatter plot of different FRUITS features $ISS_w(x)_T$ for different words w , where x is a time series from the dataset ChlorineConcentration. The plots also show histograms of the feature distribution of each single word.

ChlorineConcentration In contrast to most datasets in the UCR-archive, ChlorineConcentration (see [Li+09]) seems to be mostly unaffected by changes to the FRUITS pipeline and performs badly compared to ROCKET.

The dataset comprises 4310 time series, 467 of which are for training and 3840 are for testing. The time series length is 166. A software called EPANET was used to simulate a water distribution piping system where the concentration of chlorine in the water was measured at 166 nodes within the system. Each 5 minutes in a duration of 15 days, one such measurement was taken. This yields a total of 4310 time steps. This description is contradictory to the dataset structure. The temporal structure of a sample is given by measurements on different nodes across the piping system and not by the 4310 time steps. We believe that this labeling is responsible for the bad performance of FRUITS.

Plotting the features returned by a simple FRUITS configuration in a scatter plot⁴ results in interesting topological structures, see Figure 4. The classes in the dataset are recorded time series for different concentrations of chlorine in the water. The classes 2 and 3 are distributed on ring-like structures while the first class seems to be more scattered.

GesturePebbleZ1/2 The datasets GesturePebbleZ1 and GesturePebbleZ2 motivate the replacement of missing values in the time series with the last observed value. We compare two settings: replacing NaN (not-a-number) entries in the time series by 0 and replacing them by the last recorded (non-NaN) value. In both cases we use features $ISS_w^{S_R, W}(INC(x))_N$ for words w of weight ≤ 4 and the weighting control function $h^{(L1)}$, see (8). If NaN values appear at the start of the time series, the last recorded value is defined to be 0. The first setting produced an accuracy of 15.82% while the second one yields 29.75%. If we do not use the INC preparateur, the accuracies are 15.82% and 48.10% respectively.

PigCVP/PigArtPressure/PigAirwayPressure These datasets are presented in [GD17], where the authors had the goal to classify a three-dimensional time series as being vital signals from different pigs before or after an internal bleeding occurred. In the UCR archive, the dimensions are split into three independent datasets and the classification task is now to predict from which of the 52 different pigs one sample originates. For that, one time series is cut in three equivalently sized parts, one for the training set and two for the test set. As there are two time series for each pig, before and after internal bleeding, the datasets have 104 training samples and 208 test samples in the UCR version. The starting points of the time series at $t = 1$ in the training and test set therefore have a different meaning. Again, this dataset surfaced in our experiments as different FRUITS configurations did not perform well, in contrast to ROCKET. Intuitively, finding time series in the test set that extend the ones in the training set might be more of a pattern-matching task, which ROCKET essentially is suited best for.

Yoga This dataset of image-derived time series records distances of a persons outline to its body center while the person is doing different yoga poses. The goal here is to distinguish between a male and female person doing the same poses. Here, using just $NPI(ISS_{[14]}^{S_R}(INC(x)))$ as a feature in a

⁴All scatter plots and critical difference diagrams were made using the code publicly available at <https://github.com/irkri/classically>.

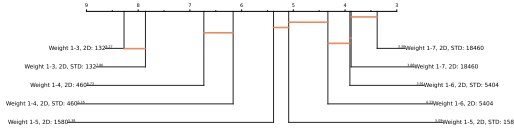


Figure 5: Critical difference diagram of fruits with and without standardization for increasing maximum word weight. Each label of a fruit also contains the total number of features used in this configuration. For example, the fruit with weight 1-5 yields 1580 features.

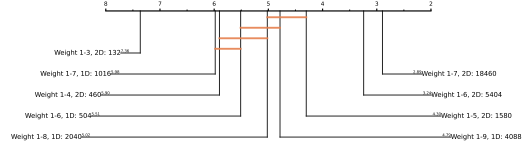


Figure 6: Comparison of fruits using a one or two-dimensional time series as input. The one dimensional version has the original time series and its increments processed separately. The two-dimensional version uses $\text{INC}^\uparrow(x)$.

linear classifier results in an accuracy of 85.37%. Another fruit calculating 300 features using words of weight 1-4 and END with ten different coquantiles on both x and $\text{INC}^\uparrow(x)$ only achieves 69.77%.

4.2 General-Purpose Fruit

The following subsections will outline our process of finding a collection of FRUITS components with their corresponding best working configuration. We decide this based on accuracy on the UCR archive as well as the compute time needed by these pipelines.

The resulting pipeline is described by the following three sequences of components, whose output is put into a linear Ridge regression classifier.

- $\text{INC}^\uparrow \rightarrow \text{STD} \rightarrow \{\text{ISS}_w^{\mathcal{S}_R, \omega} \mid |w| \leq 6\} \rightarrow \mathcal{S}$
- $\text{INC}^\uparrow \rightarrow \{\text{ISS}_w^{\mathcal{S}_A} \mid w = \underbrace{[a^{\pm 1}][b^{\mp 1}][a^{\pm 1}] \dots}_{\text{length 48}}, a, b \in \{1, 2\}\} \rightarrow \mathcal{S}$
- $\text{INC}^\uparrow \rightarrow \text{STD} \rightarrow \{\text{ISS}_w^{\omega_f^{\cos^1}}, \text{ISS}_w^{\omega_f^{\cos^2}} \mid |w| \leq 4, f \in \{i/20 \mid i = 1, 3, 5, 7, 9\}\} \rightarrow \mathcal{S}$

For the set of sieves, we use for each of the three ISS

$$\mathcal{S} = \{\text{NPI}_{\frac{1}{2}, 1}^0, \text{NPI}_{\frac{1}{2}, 1}^1, \text{NPI}_{\frac{1}{2}, 1}^2, \text{MPI}_{\frac{1}{2}, 1}^0, \text{MPI}_{\frac{1}{2}, 1}^1, \text{MPI}_{\frac{1}{2}, 1}^2, \text{END}\}.$$

4.2.1 Preparation

We examine the impact of standardizing input time series on the performance of various *fruits*, our name for complete pipelines. As illustrated in Figure 5, we employ a critical difference diagram, following [Dem06], to rank and compare the accuracy of each fruit configuration across all datasets in the UCR archive. In this diagram, configurations are ranked based on their average accuracy, with lower ranks indicating higher accuracy. To assess the statistical significance of the differences in performance, it uses two-sided Wilcoxon signed-rank tests, applying a Bonferroni-Holm correction to account for multiple comparisons. The diagram visually represents non-significant differences by connecting the respective fruits with a line. It is important to note that the expressiveness of these lines decreases as the number of compared configurations increases, due to the adjusted significance levels required by the Bonferroni-Holm correction.

Figure 5 shows that a standardized input leads to better results in all configurations. This might not be a significant difference, but it also closes the gap between the next higher total weight of words used. For example, a fruit with words of weight up to 6 are with prior standardization not significantly different to a configuration with weight 7.

Figure 6 compares the influence of the INC^\uparrow transform (9) to the one dimensional version, where the input time series and its increments are processed separately. In two dimensions, words like $[1][2]$ can be used to mix the two signals. The plot shows that words of maximum weight 5 in two dimensions surpass a configuration with maximum weight 9 in one dimension, while also being considerably smaller in feature size.

4.2.2 ISS Configurations

Weighting Section 2.4 introduces different weightings on the ISS. An open question is what weighting function h (7) to pick. We set the scaling function $f(x) = 50x$ and compare

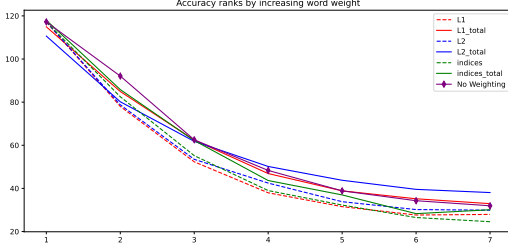


Figure 7: Ranks for the standard semiring \mathbb{S}_R .

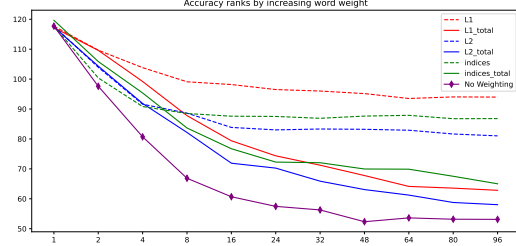


Figure 8: Ranks for the arctic semiring \mathbb{S}_A .

Average ranks of fruits with different ISS weightings for increasing word weight on the UCR archive (lower rank is better). Labels are for the corresponding weighting h and an additional “_total” is appended if the weighting is for $\alpha_p \neq 0$.

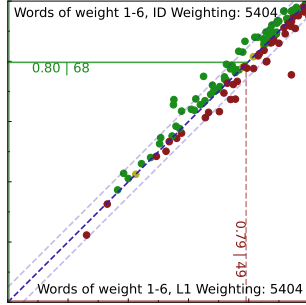


Figure 9: Comparison of $h^{(id)}$ and $h^{(L1)}$ in \mathbb{S}_R with words of weight one to six.

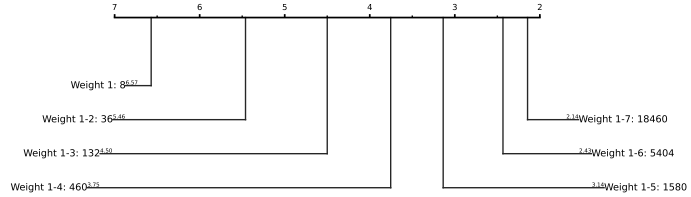


Figure 10: Critical difference diagram of different word weights for the weighting function $h^{(id)}$.

$h^{(L1)}$, $h^{(L2)}$, $h^{(id)}$ for different weights of words in Figure 7. Additionally, we experiment if the weighting for the total iterated sum $e^{t_p - T}$ has an influence in accuracy. It turns out that for \mathbb{S}_R , we get better results without this outer weighting, i.e. setting $\alpha_p = 0$ in (6). We see that in the standard semiring \mathbb{S}_R , the L1 penalization seems like the best choice for accuracy. However, as it is very close to the performance of just the indices, i.e. $h^{(id)}$, this seems to be a more natural and computational efficient choice. In the arctic semiring \mathbb{S}_A (Figure 8), no weighting seems to work best. We have to note that these plots may not be the perfect way of deciding the best configurations, as they only allow comparing the average rank of classifiers over the whole UCR archive. Zooming in on one such comparison, namely $h^{(id)}$ and $h^{(L1)}$, Figure 9 reveals the detailed differences, where $h^{(id)}$ surpasses $h^{(L1)}$ on 68 out of 128 datasets.

Words Figure 7 and 8 both also help us to decide at which word weight to cut the ISS off. For \mathbb{S}_R , weight 6 seems like a good candidate as the rank is not changing much to weight 7. This is also shown in the critical difference diagram of the word weights, see Figure 10. Each weight actually increases the accuracies significantly, but the ranks of 6 and 7 are much closer together. The time needed to compute weight 7 does not justify its use for longer time series. In the arctic semiring \mathbb{S}_A we will use words with alternating exponents $[1^{+1}][1^{-1}][1^{+1}] \dots$ and $[1^{-1}][1^{+1}][1^{-1}] \dots$ up to length 48. All of these experiments are made on two-dimensional time series $\text{INC}^\uparrow(x)$, so we actually use the alternating counterparts of the words $[1][1][1] \dots$, $[2][2][2] \dots$ as well as $[1][2][1] \dots$ and $[2][1][2] \dots$ for mixing the input time series and its increments.

Cosine Weighting Our standard configuration for a cosine weighted ISS is using words up to weight 4 (with $\alpha_1 = \dots = \alpha_p = 1$) and 10 frequencies f (compare Section 2.4). For a single cosine weighted iterated sum of length 3, we have to compute 9 iterated sums. Increasing the number of frequencies therefore is a large increase in compute time needed.

Not only is the number of frequencies used important, but also their range. A frequency parameter $f = 0.9$ corresponds to a “kernel spacing” of 90% of the time series length. Figure 11 shows that the set $\mathcal{F} = \{\frac{i}{20} \mid i = 1, \dots, 10\}$ gives the best overall results on the UCR archive out of the four tested. It performs better than also using values $f > 0.5$.

With this set \mathcal{F} , we can further reduce the number of frequencies to 5 ($\{\frac{i}{20} \mid i = 1, 3, 5, 7, 9\}$). The mean of absolute differences in accuracy of the two pipelines is $\approx 1.1\%$, while using 5 frequencies

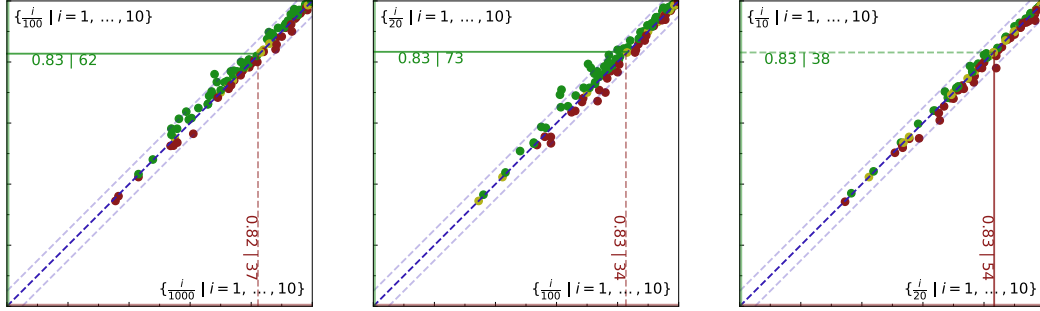


Figure 11: Comparison of four possible sets $\mathcal{F} \subset (0, 1]$ for the frequency parameter $f \in \mathcal{F}$.

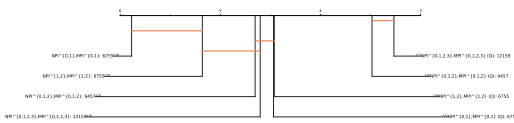


Figure 12: Standard semiring \mathbb{S}_R

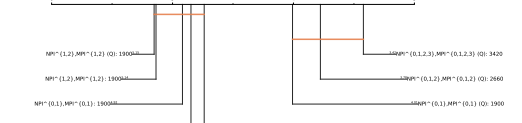


Figure 13: Arctic semiring \mathbb{S}_A

Critical Difference Diagram of various combinations of feature sieves. Each configuration also uses the END sieve, which is omitted in the description. Fruits marked with a (Q) use quantiles estimated from the training set.

being twice as fast as using 10. In practice, this can mean a speed-up of about 2000 seconds on large datasets in the UCR archive.

4.2.3 Feature Sieve Selection

We presented three feature sieves in Section 3.3. As a default, we will use for all pipelines in total seven variations of them. NPI and MPI will use quantiles for $\alpha_l = 0.5$, $\alpha_r = 1.0$ and will be evaluated on the pure iterated sums, its increments, and its second order increments. The final sieves are

$$\text{NPI}_{\frac{1}{2},1}^0, \text{NPI}_{\frac{1}{2},1}^1, \text{NPI}_{\frac{1}{2},1}^2, \text{MPI}_{\frac{1}{2},1}^0, \text{MPI}_{\frac{1}{2},1}^1, \text{MPI}_{\frac{1}{2},1}^2, \text{END}.$$

Figure 12 compare various combinations of these sieves in \mathbb{S}_R . All sieves above combined achieve a large increase in accuracy compared to reduced versions. Additionally using the third increments $\text{NPI}^3, \text{MPI}^3$ doesn't lead to a significantly better pipeline, while dramatically increasing feature count. A similar result can be observed in Figure 13 for \mathbb{S}_A . We will here settle for the same feature set.

4.3 Time warping invariance

The FRUITS pipeline built in Section 4.2 is not time warping invariant. Several components discussed before are not invariant to stuttering. For \mathbb{S}_R , we need to calculate iterated sums on the increments $\text{INC}(x)$ of the input time series. For \mathbb{S}_A , we cannot use INC , as the maximum is already invariant to repetitions of values.

As a weighting control function, we can use $h^{(L1)}$, but not $h^{(id)}$ (Section 2.4). A weighting will again only be used for \mathbb{S}_R . Features of cosine weighted iterated sums are not time warping invariant.

The only feature sieves discussed so far that are time warping invariant are $\text{NPI}^1, \text{MPI}^1$ and END . The resulting time-warping invariant pipeline is:

- $\text{INC} \rightarrow \{\text{ISS}_w^{\mathbb{S}_R, \omega} \mid |w| \leq 9\} \rightarrow \text{NPI}^1, \text{MPI}^1, \text{END}$
- $\{\text{ISS}_w^{\mathbb{S}_A} \mid w = \underbrace{[1^{\pm 1}][1^{\mp 1}][1^{\pm 1}] \dots}_{\text{length 48}}\} \rightarrow \text{NPI}^1, \text{MPI}^1, \text{END}$

Figure 11 shows results of experiments comparing different magnitudes of stuttering. For that, the training set of any dataset in the UCR archive was left unchanged. The linear classifier was fit on

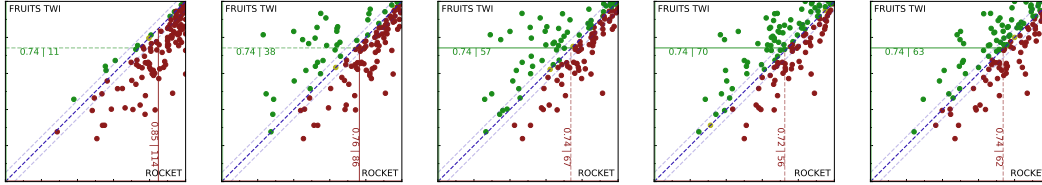


Figure 14: Comparisons of FRUITS to ROCKET for an increasing magnitude of time series stuttering. From left-to-right the proportional additional lengths are 0%, 10%, 20%, 50% and 90%. FRUITS TWI marks the time warping invariant pipeline.

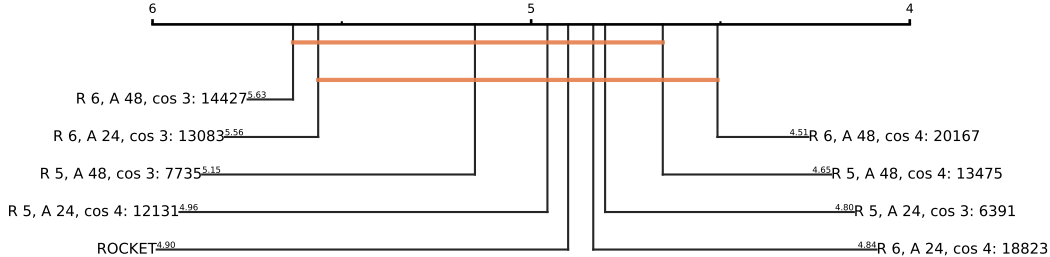


Figure 15: Critical Difference Diagram of fruits with slightly different words for the ISS. The name of one configuration tells us the maximum weight of words in S_R , the length of words in S_A , and the maximum weight used with cosine weighted ISS. ROCKET is right in the center of this comparison.

the computed features and then tested on features of a stuttered version of the test set. We varied the amount of time points added to the time series. The positions where stuttering occurred are random. ROCKET is not naturally able to deal with inputs of different lengths in the training and test set. For experiments with ROCKET, we therefore also lengthen the time series in the training set by the same amount as the test set by repeating the last value a fixed number of times. The results show that ROCKET’s accuracy deteriorates quite quickly even for slightly stuttered time series, while the features of FRUITS are identical in these experiments.

IMU Data for Point of Impact Localization An earlier version of FRUITS (only available as an open-source GitHub repository) was already used to classify a novel dataset in robotics [KE22]. The involved time series are recordings of an inertial measurement unit (IMU) during collision of a robot with an obstacle. The recorded variables were linear acceleration and rotational velocity in three dimensions. With that, one time series is six dimensional. On this dataset, FRUITS can compete with ROCKET, even when choosing a small pipeline that is significantly faster than ROCKET. The IMU data is a good example of a practical application of time-warping invariance. The time of the collision is unknown, and right before it, the robot has nearly constant acceleration and rotational velocity. This time interval can be interpreted to be a sequence of stuttered values.

4.4 A reduced pipeline

Although being very competitive with SOTA methods, the FRUITS configuration found in Section 4.2 is heavy on number of features and the pipeline is a bit slower than ROCKET. We conducted a wide range of experiments changing the maximum weight $|w|$ of words w used in this Fruit. Figure 15 shows some of the best alternatives we tested. Interestingly, restricting the weight of words for each type of ISS leads to a very good pipeline, competing with our choice from Section 4.2. Figure 16 presents the scatter plot of ROCKET, our general purpose Fruit and its reduced version.

5 Outlook

- Our python package, <https://github.com/irkri/fruits>, is object-oriented and modular, thereby easily extensible and readable. It uses numba’s [LPS15] JIT capabilities in parts, but is not fully optimized. For example, parallelization over training examples is interrupted at each of the three steps in FRUITS. Grouping them in one function can lead to a significant speed-up.

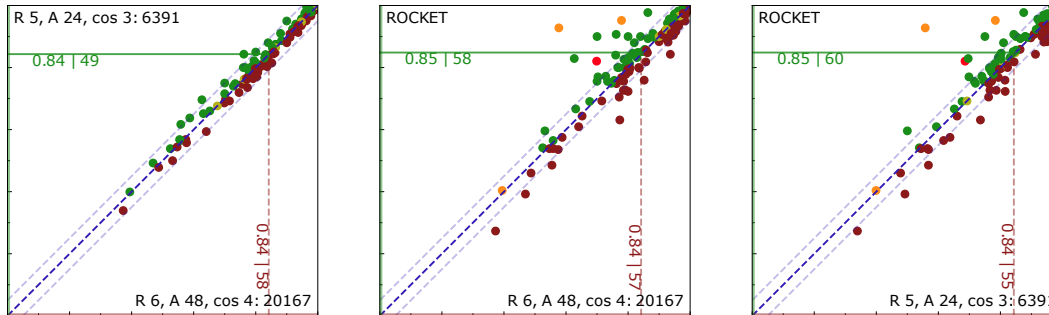


Figure 16: Detailed comparison of fruits from Figure 15. The orange points of the two right comparisons mark the datasets PigCVP, PigArt-Pressure and PigAirwayPressure; the bright red point is ChlorineConcentration (see Section 4.1).

- Although the calculation of the argmax indices, which we propose here for the first time and whose algorithm is given is Algorithm 1, leads to a general improvement of classification accuracy, we believe that the full potential of this feature has not yet been exploited.
- The coquantile-features, although theoretically sounds, does *not* lead to an improvement of classification accuracy. Nonetheless we believe that this feature has potential and should be further investigated. Similarly, it would be interesting to see if features obtained via the Bayesian semiring lead to an improvement of classification accuracy.
- In this work we have demonstrated that the iterated-sums signature can be used as a feature-extraction method for time series classification. The natural next step is to use it as a *trainable layer* in a neural network.
- Certain terms of the iterated-sums signature are interpretable either as cross-correlations of the time series or as certain geometric features of the time series, [DR19]. It would be interesting to make use of this fact in the context of our pipeline.

Acknowledgments J. Diehl was supported by a Trilateral ANR-DFG-JST AI program, DFG Project 442590525. J. Diehl and R. Krieg were supported by the project “Signatures for Images” at the Centre for Advanced Study at the Norwegian Academy of Science and Letters in Oslo, Norway, during the academic year 2023/24.

References

- [Bag+18] A. Bagnall, H. A. Dau, J. Lines, M. Flynn, J. Large, A. Bostrom, P. Southam, and E. Keogh. “The UEA multivariate time series classification archive, 2018”. In: *arXiv preprint arXiv:1811.00075* (2018). URL: <https://arxiv.org/abs/1811.00075>.
- [Bag+17] A. Bagnall, J. Lines, A. Bostrom, J. Large, and E. Keogh. “The great time series classification bake off: a review and experimental evaluation of recent algorithmic advances”. In: *Data mining and knowledge discovery* 31 (2017), pp. 606–660.
- [BC94] D. J. Berndt and J. Clifford. “Using dynamic time warping to find patterns in time series”. In: *Proceedings of the 3rd international conference on knowledge discovery and data mining*. 1994, pp. 359–370.
- [Che57] K.-T. Chen. “Integration of paths, geometric invariants and a generalized Baker-Hausdorff formula”. In: *Annals of Mathematics* 65.1 (1957), pp. 163–178.
- [CNO18] I. Chevyrev, V. Nanda, and H. Oberhauser. “Persistence paths and signature features in topological data analysis”. In: *IEEE transactions on pattern analysis and machine intelligence* 42.1 (2018), pp. 192–202.
- [Cuc+21] C. Cuchiero, L. Gonon, L. Grigoryeva, J.-P. Ortega, and J. Teichmann. “Expressive power of randomized signature”. In: *The Symbiosis of Deep Learning and Differential Equations*. 2021.
- [CB17] M. Cuturi and M. Blondel. “Soft-dtw: a differentiable loss function for time-series”. In: *International conference on machine learning*. PMLR. 2017, pp. 894–903.

- [Dau+19] H. A. Dau, A. Bagnall, K. Kamgar, C.-C. M. Yeh, Y. Zhu, S. Gharghabi, C. A. Ratanamahatana, and E. Keogh. “The UCR time series archive”. In: *IEEE/CAA Journal of Automatica Sinica* 6.6 (2019), pp. 1293–1305. URL: <https://ieeexplore.ieee.org/abstract/document/8894743>.
- [DET20] J. Diehl, K. Ebrahimi-Fard, and N. Tapia. “Time-warping invariants of multidimensional time series”. In: *Acta Applicandae Mathematicae* 170.1 (2020), pp. 265–290.
- [DET22] J. Diehl, K. Ebrahimi-Fard, and N. Tapia. “Tropical Time Series, Iterated-Sums Signatures, and Quasisymmetric Functions”. In: *SIAM Journal on Applied Algebra and Geometry* 6.4 (2022), pp. 563–599.
- [Dem06] J. Demšar. “Statistical comparisons of classifiers over multiple data sets”. In: *The Journal of Machine Learning Research* 7 (2006), pp. 1–30.
- [DSW23] A. Dempster, D. F. Schmidt, and G. I. Webb. “Hydra: Competing convolutional kernels for fast and accurate time series classification”. In: *Data Mining and Knowledge Discovery* (2023), pp. 1–27.
- [DR19] J. Diehl and J. Reizenstein. “Invariants of multidimensional time series based on their iterated-integral signature”. In: *Acta Applicandae Mathematicae* 164.1 (2019), pp. 83–122.
- [DPW20] A. Dempster, F. Petitjean, and G. I. Webb. “ROCKET: exceptionally fast and accurate time series classification using random convolutional kernels”. In: *Data Mining and Knowledge Discovery* 34.5 (2020), pp. 1454–1495.
- [DSW21] A. Dempster, D. F. Schmidt, and G. I. Webb. “MINIROCKET: A Very Fast (Almost) Deterministic Transform for Time Series Classification”. en. In: *Proceedings of the 27th ACM SIGKDD Conference on Knowledge Discovery & Data Mining*. arXiv:2012.08791 [cs, stat]. Aug. 2021, pp. 248–257. DOI: 10.1145/3447548.3467231. URL: <http://arxiv.org/abs/2012.08791>.
- [Fli81] M. Fliess. “Fonctionnelles causales non linéaires et indéterminées non commutatives”. In: *Bulletin de la société mathématique de France* 109 (1981), pp. 3–40.
- [FMZ21] L. Foissy, D. Manchon, and Y. Zhang. “A general construction of family algebraic structures”. In: (2021).
- [GD17] M. Guillaume-Bert and A. Dubrawski. “Classification of time sequences using graphs of temporal constraints”. In: *The Journal of Machine Learning Research* 18.1 (2017), pp. 4370–4403.
- [Hof00] M. E. Hoffman. “Quasi-shuffle products”. In: *Journal of Algebraic Combinatorics* 11.1 (2000), pp. 49–68.
- [Ism+19] H. Ismail Fawaz, G. Forestier, J. Weber, L. Idoumghar, and P.-A. Muller. “Deep learning for time series classification: a review”. In: *Data mining and knowledge discovery* 33.4 (2019), pp. 917–963.
- [KMN08] A. Kampouraki, G. Manis, and C. Nikou. “Heartbeat time series classification with support vector machines”. In: *IEEE transactions on information technology in biomedicine* 13.4 (2008), pp. 512–518.
- [KR05] E. Keogh and C. A. Ratanamahatana. “Exact indexing of dynamic time warping”. In: *Knowledge and information systems* 7 (2005), pp. 358–386.
- [Kid+19] P. Kidger, P. Bonnier, I. Perez Arribas, C. Salvi, and T. Lyons. “Deep signature transforms”. In: *Advances in Neural Information Processing Systems* 32 (2019).
- [Kid+20] P. Kidger, J. Morrill, J. Foster, and T. Lyons. “Neural controlled differential equations for irregular time series”. In: *Advances in Neural Information Processing Systems* 33 (2020), pp. 6696–6707.
- [KO19] F. J. Király and H. Oberhauser. “Kernels for sequentially ordered data”. In: *Journal of Machine Learning Research* 20 (2019).
- [Kou+14] J. Koutník, K. Greff, F. Gomez, and J. Schmidhuber. “A clockwork rnn”. In: *International conference on machine learning*. PMLR. 2014, pp. 1863–1871.
- [Kri21] R. Krieg. “Klassifikation von Zeitreihen mithilfe iterierter Summen”. Bachelor’s Thesis. Universität Greifswald, 2021. URL: <https://github.com/alienkrieg/fruits/releases/tag/v0.9.2>.

- [KE22] R. Krieg and M. Ebner. “Time Series Classification of IMU Data for Point of Impact Localization”. In: *2022 Sixth IEEE International Conference on Robotic Computing (IRC)*. IEEE. 2022, pp. 93–94.
- [LPS15] S. K. Lam, A. Pitrou, and S. Seibert. “Numba: A llvm-based python jit compiler”. In: *Proceedings of the Second Workshop on the LLVM Compiler Infrastructure in HPC*. 2015, pp. 1–6.
- [Li+09] L. Li, J. McCann, N. S. Pollard, and C. Faloutsos. “Dynammo: Mining and summarization of coevolving sequences with missing values”. In: *Proceedings of the 15th ACM SIGKDD international conference on Knowledge discovery and data mining*. 2009, pp. 507–516.
- [Lön+19] M. Löning, A. Bagnall, S. Ganesh, V. Kazakov, J. Lines, and F. J. Király. “sktime: A unified interface for machine learning with time series”. In: *arXiv preprint arXiv:1909.07872* (2019). URL: <https://github.com/sktime/sktime>.
- [Lyo98] T. J. Lyons. “Differential equations driven by rough signals”. In: *Revista Matemática Iberoamericana* 14.2 (1998), pp. 215–310.
- [McC18] P. McCullagh. *Tensor methods in statistics*. Courier Dover Publications, 2018.
- [Mid+21] M. Middlehurst, J. Large, M. Flynn, J. Lines, A. Bostrom, and A. Bagnall. “HIVE-COTE 2.0: a new meta ensemble for time series classification”. In: *Machine Learning* 110.11 (2021), pp. 3211–3243.
- [Moh+02] M. Mohri et al. “Semiring frameworks and algorithms for shortest-distance problems”. In: *Journal of Automata, Languages and Combinatorics* 7.3 (2002), pp. 321–350.
- [MSB23] M. Middlehurst, P. Schäfer, and A. Bagnall. “Bake off redux: a review and experimental evaluation of recent time series classification algorithms”. In: *arXiv:2304.13029* (Apr. 2023). URL: <http://arxiv.org/abs/2304.13029>.
- [MSS13] M. Mubashir, L. Shao, and L. Seed. “A survey on fall detection: Principles and approaches”. In: *Neurocomputing* 100 (2013), pp. 144–152.
- [Qin+21] Z. Qin, W. Sun, H. Deng, D. Li, Y. Wei, B. Lv, J. Yan, L. Kong, and Y. Zhong. “cosFormer: Rethinking Softmax In Attention”. In: *International Conference on Learning Representations*. 2021.
- [Tan+22] C. W. Tan, A. Dempster, C. Bergmeir, and G. I. Webb. “MultiRocket: multiple pooling operators and transformations for fast and effective time series classification”. In: *Data Mining and Knowledge Discovery* 36.5 (2022), pp. 1623–1646.
- [Vas+17] A. Vaswani, N. Shazeer, N. Parmar, J. Uszkoreit, L. Jones, A. N. Gomez, Ł. Kaiser, and I. Polosukhin. “Attention is all you need”. In: *Advances in neural information processing systems* 30 (2017).
- [WYO17] Z. Wang, W. Yan, and T. Oates. “Time series classification from scratch with deep neural networks: A strong baseline”. In: *2017 International joint conference on neural networks (IJCNN)*. IEEE. 2017, pp. 1578–1585.
- [Xie+17] Z. Xie, Z. Sun, L. Jin, H. Ni, and T. Lyons. “Learning spatial-semantic context with fully convolutional recurrent network for online handwritten chinese text recognition”. In: *IEEE transactions on pattern analysis and machine intelligence* 40.8 (2017), pp. 1903–1917.
- [YJF98] B.-K. Yi, H. V. Jagadish, and C. Faloutsos. “Efficient retrieval of similar time sequences under time warping”. In: *Proceedings 14th International Conference on Data Engineering*. IEEE. 1998, pp. 201–208.
- [Zah+17] M. Zaheer, S. Kottur, S. Ravanbakhsh, B. Poczos, R. R. Salakhutdinov, and A. J. Smola. “Deep sets”. In: *Advances in neural information processing systems* 30 (2017).
- [Zhe+14] Y. Zheng, Q. Liu, E. Chen, Y. Ge, and J. L. Zhao. “Time series classification using multi-channels deep convolutional neural networks”. In: *International conference on web-age information management*. Springer. 2014, pp. 298–310.

A Iterated-sums signature

Let $A = \{1, \dots, d\}$ be an alphabet whose elements represent dimension indices. Consider the free commutative monoid \mathcal{A} over it, consisting of all commutative monomials in the generators A . We

denote the empty word by e and, enclose, for readability, the elements of \mathcal{A} in brackets, e.g. for $d = 3$,

$$e, [1^3 3^5], [123], [2^7] \in \mathcal{A}.$$

For a field \mathbb{K} , we then consider the tensor \mathbb{K} -algebra over \mathcal{A}

$$\mathcal{T}(\mathcal{A}) = \bigoplus_{n \geq 0} \mathbb{K}[\mathcal{A}]^{\otimes n} \cong \mathbb{K}e \oplus \left(\bigoplus_{n \geq 1} \mathbb{K}[\mathcal{A}]^{\otimes n} \right).$$

Elements of $\mathcal{T}(\mathcal{A})$ can be considered to be *finite*, \mathbb{K} -linear combinations of words in \mathcal{A} . For example, for $d = 3$ and $\mathbb{K} = \mathbb{R}$,

$$e \in \mathbb{R}[\mathcal{A}]^{\otimes 0}, \quad -[1^3 3^5] + 17[123] + 2[2^7] \in \mathbb{R}[\mathcal{A}]^{\otimes 1}, \quad [1][1] - [1^3 3^5][123] \in \mathbb{R}[\mathcal{A}]^{\otimes 2}.$$

For a given time series $x \in \mathcal{Z}_d$ the iterated-sums signature is an element of the (algebraic) dual space of $\mathcal{T}(\mathcal{A})$. We denote the dual pairing with $\langle \cdot, \cdot \rangle$. Then, the signature on the basis elements of words in \mathcal{A} is, for $s \leq t$ defined as

$$\langle [a_1] \cdots [a_p], \text{ISS}_{s,t}(x) \rangle := \sum_{s < t_1 < \dots < t_p \leq t} x_{t_1}^{[a_1]} \cdots x_{t_p}^{[a_p]} \quad (10)$$

In the main text we use the short notation

$$\text{ISS}_w(x)_t := \langle [a_1] \cdots [a_p], \text{ISS}_{0,t}(x) \rangle.$$

Remark A.1. Note that the sum “scans” over all subsequences of x of a fixed length. Contrast this with a convolutional neural network (CNN), which only scans over consecutive subsequences. This point is further discussed in [DET22].

For example,

$$\begin{aligned} \langle [1^2], \text{ISS}_{0,3}(x) \rangle &= (x_1^{[1]})^2 + (x_2^{[1]})^2 + (x_3^{[1]})^2 \\ \langle [1^2 2][5], \text{ISS}_{0,3}(x) \rangle &= \sum_{0 < t_1 < t_2 \leq 3} x_{t_1}^{[1^2 2]} x_{t_2}^{[5]} \\ &= \sum_{0 < t_1 < t_2 \leq 3} (x_{t_1}^{[1]})^2 x_{t_1}^{[2]} x_{t_2}^{[5]} \\ &= x_1^{[1]} x_1^{[2]} x_2^{[5]} + (x_1^{[1]} x_1^{[2]} + x_2^{[1]} x_2^{[2]}) x_3^{[5]}. \end{aligned}$$

Theorem A.2.

1. (Invariance) The iterated-sums signature is invariant to insertion of zeros: let $t \leq T$ be any timepoint and let y be the time series

$$y_i := \begin{cases} x_i, & i < t \\ 0, & i = t \\ x_{i-1}, & t < i. \end{cases}$$

Then $\text{ISS}_{0,T}(x) = \text{ISS}_{0,T+1}(y)$. In particular, if x has finite support, $\text{ISS}_{0,\infty}(x) = \text{ISS}_{0,\infty}(y)$.

2. (Dynamic programming) For any word $[a_1] \dots [a_p]$,

$$\langle [a_1] \dots [a_p], \text{ISS}_{s,t}(x) \rangle = \sum_{i=s+1}^t \langle [a_1] \dots [a_{p-1}], \text{ISS}_{n,i-1}(x) \rangle x_i^{[a_p]}.$$

3. (Quasi-shuffle identity) There is a commutative product \star on $\mathcal{T}(\mathcal{A})$ such that for all elements $\phi, \psi \in \mathcal{T}(\mathcal{A})$ and all $x \in \mathcal{Z}_d$, and all $s \leq t$,

$$\langle \phi, \text{ISS}_{s,t}(x) \rangle \langle \psi, \text{ISS}_{s,t}(x) \rangle = \langle \phi \star \psi, \text{ISS}_{s,t}(x) \rangle.$$

Remark A.3.

1. The ostensibly polynomial-time algorithm for computing a term in the iterated-sums signature (after all, (10) contains $\binom{T}{p}$ terms), is reduced to a linear time algorithm by the dynamic programming property.
2. The quasi-shuffle identity implies that any polynomial expression in terms of the iterated-sums signature can be re-expressed as a linear expression in (other) terms of the signature.

B Argmax indices

A pseudo-implementation of the algorithm computing $\text{ISS}_{zw}^{\text{SA}}$, and the corresponding cumulative argmax and argmin, is shown in Algorithm 1. It is best understood by an example. Let

$$z = (1, 3, -4, 2, 0, 5, 1, 1), \quad w = [1][1^{-1}][1],$$

and consider the steps of the first for-loop,

$$\begin{array}{ll} \mathbf{k} = 1 & \mathbf{k} = 2 \\ z = (1, 3, 3, 3, 3, 5, 5, 5) & z = (0, 0, 7, 1, 3, 0, 4, 4) \\ J^{(1)} = (1, 2, 2, 2, 2, 6, 6, 6) & J^{(2)} = (1, 1, 3, 3, 3, 3, 3, 3) \end{array}$$

$$\begin{array}{l} \mathbf{k} = 3 \\ z = (1, 3, 3, 3, 3, 5, 5, 5) \\ J^{(3)} = (1, 2, 2, 2, 2, 6, 6, 6). \end{array}$$

We see that $(J_8^{(1)}, J_8^{(2)}, J_8^{(3)}) = (6, 3, 6)$, which is *not* the correct positions of the argmax of $\text{ISS}_{zw}^{\text{SA}}(z)$ (they are not even ordered correctly). The second for-loop corrects this,

$$\begin{array}{ll} \mathbf{k} = 3 & \mathbf{k} = 2 \\ J^{(2)} = (1, 1, 3, 3, 3, 3, 3, 3) \text{ (no change)} & J^{(1)} = (1, 2, 2, 2, 2, 2, 2, 2). \end{array}$$

Now at each timepoint i , $(J_i^{(1)}, J_i^{(2)}, J_i^{(3)})$ contains the correct tuple giving the argmax (up to i) of the expression $z_{t_1} - z_{t_2} + z_{t_3}$.

Algorithm 1 Implementation of the Arctic Iterated Sum with Argmax Computation

Require: $x \in \mathcal{Z}_d|_T, w = [a_1] \dots [a_p]$
 $z \leftarrow (0, 0, \dots, 0) \in \mathcal{Z}_d|_T$
 $J^{(1)}, \dots, J^{(p)} \leftarrow (1, 1, \dots, 1) \in \mathbb{N}^T$
for $k = 1, 2, \dots, p$ **do**
 $z \leftarrow z \odot x^{\odot [a_k]}$
 for $t = 2, 3, \dots, T$ **do**
 if $z_{t-1} \geq z_t$ **then**
 $z_t \leftarrow z_{t-1}$
 $J_t^{(k)} \leftarrow J_{t-1}^{(k)}$
 else
 $J_t^{(k)} \leftarrow i$
 end if
 end for
end for
for $k = p, p-1, \dots, 2$ **do** ▷ Retranslate argmax of prior steps
 $\hat{t} \leftarrow J_T^{(k)}$
 for $t = \hat{t} + 1, \hat{t} + 2, \dots, T$ **do**
 $J_t^{(k-1)} \leftarrow J_{\hat{t}}^{(k-1)}$
 end for
end for
return $J^{(1)}, \dots, J^{(p)}$

C Detailed results on the UCR archive

Table 1: Results of our general pipeline from Section 4.2, its reduced Version and ROCKET. All values are rounded to two decimal places. We ran the experiments for ROCKET on comparable hardware using the implementation in the Python package “sktime” [Lön+19].

Datensatz	FRUITS (general)	FRUITS (general)	FRUITS (reduced)	FRUITS (reduced)	ROCKET	ROCKET
	Time in s	Accuracy	Time in s	Accuracy	Time in s	Accuracy
ACSF1	103.8850	0.8200	30.7467	0.8100	68.0116	0.8800
Adiac	146.7699	0.8363	26.6219	0.8031	29.4448	0.7980
AllGestureWiimoteX	222.4712	0.7029	51.2969	0.6986	91.4391	0.7700
AllGestureWiimoteY	223.2950	0.7857	50.7273	0.7714	91.7233	0.7557
AllGestureWiimoteZ	223.0890	0.7000	50.8938	0.7157	91.4727	0.7557
ArrowHead	40.3043	0.8343	7.4897	0.8229	8.8019	0.8000
BME	33.6932	1.0000	5.4710	1.0000	3.9481	1.0000
Beef	24.9715	0.7667	5.2954	0.8000	6.1328	0.8000
BeetleFly	21.3279	0.7000	4.2534	0.7500	4.4935	0.9000
BirdChicken	21.2520	0.8000	4.2721	0.8500	4.4971	0.9000
CBF	115.4111	0.9922	18.6144	0.9889	17.4609	1.0000
Car	41.5531	0.9000	9.0585	0.9500	14.7491	0.8833
Chinatown	40.0493	0.9621	6.2121	0.9796	1.6270	0.9825
ChlorineConcentration	560.7010	0.6987	99.7959	0.6859	112.0990	0.8206
CinCECGTorso	477.1361	0.9362	137.0647	0.9130	342.4357	0.8428
Coffee	22.5474	1.0000	4.5174	1.0000	3.5598	1.0000
Computers	159.8291	0.7280	41.3156	0.7400	76.5646	0.7720
CricketX	175.3668	0.8051	39.1927	0.7821	49.5737	0.8128
CricketY	176.2559	0.8154	36.0704	0.8026	49.4597	0.8462
CricketZ	176.1705	0.8462	36.7134	0.8410	49.1782	0.8513
Crop	2513.8601	0.7559	389.2360	0.7460	244.2807	0.7589
DiatomSizeReduction	57.6231	0.9510	11.3183	0.9510	16.5017	0.9739
DistalPhalanxOutlineAgeGroup	92.7824	0.7338	15.5602	0.7482	11.0868	0.7554
DistalPhalanxOutlineCorrect	141.1326	0.7790	23.5171	0.7935	17.3493	0.7681
DistalPhalanxTW	93.3472	0.6763	15.8799	0.6763	11.1294	0.6906
DodgerLoopDay	42.4246	0.5875	8.4260	0.6375	9.6738	0.5750
DodgerLoopGame	33.3166	0.8623	6.3397	0.8478	7.2719	0.8478
DodgerLoopWeekend	33.2566	0.9855	6.3098	0.9855	7.2928	0.9710
ECG200	39.7998	0.8800	6.8275	0.9100	4.2564	0.9100
ECG5000	624.3180	0.9453	105.2711	0.9438	108.6894	0.9473
ECGFiveDays	112.1084	0.9965	18.7340	0.9884	17.3435	1.0000
EOGHorizontalSignal	307.0393	0.6519	90.9360	0.6602	193.8802	0.6436
EOGVerticalSignal	308.4106	0.5249	92.9148	0.5387	192.7934	0.5414
Earthquakes	148.7143	0.7626	35.4661	0.7626	56.7548	0.7482
ElectricDevices	2487.5423	0.7850	407.7890	0.7865	395.0014	0.7266
EthanolLevel	554.0979	0.5320	175.5845	0.5000	378.8231	0.5960
FaceAll	327.0687	0.9479	53.7708	0.9574	52.2166	0.9485
FaceFour	29.3490	0.8636	5.5186	0.8750	6.8268	0.9773
FacesUCR	284.1094	0.9532	46.9586	0.9527	45.2283	0.9624
FiftyWords	194.5440	0.8022	39.0089	0.7934	51.6230	0.8330
Fish	93.3825	0.9943	21.5958	0.9886	34.2483	0.9829
FordA	1529.9502	0.9341	363.5169	0.9295	606.4828	0.9326
FordB	1456.3689	0.7914	344.5664	0.7642	574.2988	0.7975
FreezerRegularTrain	426.4477	0.9975	84.6967	0.9975	133.4468	0.9975
FreezerSmallTrain	395.0881	0.9646	78.3031	0.9653	122.1863	0.9495
Fungi	36.0511	0.9946	6.3441	0.9892	6.4146	1.0000
GestureMidAirD1	87.5611	0.8000	18.2568	0.8154	27.7108	0.7231
GestureMidAirD2	87.4361	0.7154	18.0444	0.6923	27.6469	0.6923
GestureMidAirD3	87.5339	0.4692	18.0728	0.4923	27.8279	0.3923
GesturePebbleZ1	77.2623	0.7616	16.6545	0.8430	28.0296	0.9070
GesturePebbleZ2	79.2145	0.6266	17.2571	0.6962	28.9427	0.8291
GunPoint	39.0924	1.0000	6.6252	1.0000	5.3985	1.0000
GunPointAgeSpan	75.8172	1.0000	12.8286	1.0000	12.5102	0.9968
GunPointMaleVersusFemale	75.7960	0.9937	12.9539	0.9968	12.5354	1.0000
GunPointOldVersusYoung	76.0313	1.0000	13.0708	1.0000	12.5133	0.9937
Ham	58.3094	0.7714	12.8599	0.7619	19.7050	0.7048
HandOutlines	1806.0411	0.9270	438.1933	0.9270	924.9054	0.9432
Haptics	164.0699	0.5747	46.0450	0.5682	95.7822	0.5357
Herring	41.9130	0.6406	9.3133	0.5938	14.0290	0.6094
HouseTwenty	85.6755	0.9580	26.3777	0.9748	56.8769	0.9664
InlineSkate	273.4654	0.4873	85.2718	0.4782	201.7249	0.4600
InsectEPGRegularTrain	75.6846	1.0000	17.4847	1.0000	31.6752	1.0000
InsectEPGSmallTrain	59.5023	0.9639	13.8049	0.9960	24.0207	0.9719
InsectWingbeatSound	317.7948	0.6313	60.8058	0.6515	86.4057	0.6667
ItalyPowerDemand	98.8642	0.9572	14.2100	0.9582	4.6215	0.9699
LargeKitchenAppliances	228.1177	0.8640	58.9839	0.8640	114.5984	0.8933
Lightning2	43.1336	0.8033	10.0242	0.7705	16.3494	0.7869
Lightning7	39.2630	0.7945	7.8351	0.8219	9.6539	0.8082
Mallat	563.9630	0.9680	150.3094	0.9706	357.6235	0.9561
Meat	38.7542	0.9833	8.1664	0.9833	11.4819	0.9500
MedicalImages	154.3396	0.8066	25.2166	0.7855	21.5492	0.7974
MelbournePedestrian	376.5571	0.9463	53.5563	0.9504	19.9616	0.9041
MiddlePhalanxOutlineAgeGroup	94.6831	0.5584	15.7533	0.6169	11.2054	0.5649
MiddlePhalanxOutlineCorrect	142.0556	0.8316	23.2861	0.8419	17.4664	0.8488
MiddlePhalanxTW	94.4105	0.5584	16.0048	0.5649	11.2662	0.5390
MixedShapesRegularTrain	809.0065	0.9810	221.4802	0.9827	500.0832	0.9687

MixedShapesSmallTrain	598.9045	0.9468	161.0292	0.9526	381.6234	0.9398
MoteStrain	124.4697	0.9185	19.6880	0.9241	15.5286	0.9161
NonInvasiveFetalECGThorax1	1180.2862	0.9328	303.2314	0.9201	596.2126	0.9562
NonInvasiveFetalECGThorax2	1175.7718	0.9481	307.1615	0.9394	592.4068	0.9695
OSULeaf	111.1544	0.9628	24.0269	0.9504	38.5401	0.9339
OliveOil	25.9721	0.9333	5.5478	0.9333	7.3465	0.9000
PLAID	461.1692	0.9106	136.6596	0.8976	308.7824	0.8957
PhalangesOutlinesCorrect	406.6570	0.8287	68.7272	0.8310	52.7301	0.8322
Phoneme	539.0527	0.3729	151.8750	0.3391	338.6129	0.2732
PickupGestureWiimoteZ	32.3531	0.7600	6.3494	0.8000	7.7745	0.8400
PigAirwayPressure	166.8228	0.3942	54.7703	0.3990	119.4694	0.4038
PigArtPressure	166.7602	0.7788	54.0380	0.7837	119.5880	0.9519
PigCVP	168.4422	0.5769	54.1686	0.5577	119.5621	0.9279
Plane	46.1604	1.0000	8.0256	1.0000	6.5593	1.0000
PowerCons	70.9078	0.9667	12.3003	0.9722	11.1062	0.9444
ProximalPhalanxOutlineAgeGroup	98.7970	0.8537	16.6446	0.8634	11.8470	0.8585
ProximalPhalanxOutlineCorrect	141.8519	0.8832	22.5560	0.8866	17.4980	0.8969
ProximalPhalanxTW	98.9089	0.7707	15.7628	0.7659	11.8203	0.8000
RefrigerationDevices	236.6392	0.5467	59.1469	0.5440	114.6262	0.5387
Rock	58.7814	0.9000	17.2947	0.8800	36.9936	0.9000
ScreenType	231.0993	0.5547	56.4944	0.5680	114.7023	0.4853
SemgHandGenderCh2	385.7292	0.9467	112.4464	0.9350	256.8057	0.9333
SemgHandMovementCh2	440.6971	0.7733	130.2039	0.7356	289.6836	0.6311
SemgHandSubjectCh2	443.0387	0.9289	132.1427	0.9400	288.8713	0.8822
ShakeGestureWiimoteZ	32.7251	0.8400	6.3978	0.8800	8.3014	0.9000
ShapeletSim	45.7352	0.9778	9.7770	0.9667	15.4871	1.0000
ShapesAll	315.8352	0.9100	74.4450	0.9083	129.5974	0.9067
SmallKitchenAppliances	229.5016	0.7867	61.1253	0.8027	114.3987	0.8267
SmoothSubspace	44.5609	0.9800	6.9869	0.9800	1.3466	0.9800
SonyAIBORobotSurface1	63.1918	0.9351	10.5504	0.9318	6.5557	0.9201
SonyAIBORobotSurface2	93.0693	0.9538	15.1537	0.9486	9.5274	0.9161
StarLightCurves	3453.7035	0.9828	1007.1417	0.9815	1491.4362	0.9809
Strawberry	219.1153	0.9730	43.6401	0.9676	53.1089	0.9811
SwedishLeaf	190.8527	0.9664	32.8953	0.9632	29.6483	0.9664
Symbols	159.5754	0.9779	34.0788	0.9869	58.6279	0.9739
SyntheticControl	85.6283	0.9867	14.0725	0.9833	8.1304	1.0000
ToeSegmentation1	49.9530	0.9474	9.7132	0.9474	12.0201	0.9605
ToeSegmentation2	37.6048	0.9231	7.6487	0.9154	9.8929	0.9231
Trace	49.9922	1.0000	9.8723	1.0000	11.7620	1.0000
TwoLeadECG	113.2748	0.9991	18.3285	0.9982	13.9761	0.9991
TwoPatterns	687.6013	1.0000	116.4858	1.0000	109.3184	1.0000
UMD	34.1950	0.9792	6.0866	0.9861	4.6954	0.9931
UWaveGestureLibraryAll	1513.8865	0.9782	428.2773	0.9785	719.8314	0.9749
UWaveGestureLibraryX	748.4149	0.8582	155.4899	0.8504	239.3662	0.8562
UWaveGestureLibraryY	745.8251	0.7929	156.2063	0.7769	237.7104	0.7781
UWaveGestureLibraryZ	744.7869	0.7990	153.7822	0.7968	238.0823	0.7942
Wafer	949.0571	0.9997	165.2583	0.9997	175.5310	0.9987
Wine	32.6485	0.8519	6.0274	0.8148	5.6719	0.7593
WordSynonyms	164.4819	0.7461	32.4855	0.7194	44.4603	0.7492
Worms	115.2875	0.7922	32.0435	0.7662	56.1034	0.7273
WormsTwoClass	114.5489	0.8571	31.9260	0.8442	56.4634	0.8182
Yoga	552.3818	0.9387	121.8544	0.9350	215.9253	0.9103